

Neutrino Scattering in Heterogeneous Supernova Plasmas

O.L. Caballero* and C.J. Horowitz†

Department of Physics and Nuclear Theory Center, Indiana University, Bloomington, IN 47405

D. K. Berry‡

University Information Technology Services, Indiana University, Bloomington, IN 47408

(Dated: April 26, 2018)

Neutrinos in core collapse supernovae are likely trapped by neutrino-nucleus elastic scattering. Using molecular dynamics simulations, we calculate neutrino mean free paths and ion-ion correlation functions for heterogeneous plasmas. Mean free paths are systematically shorter in plasmas containing a mixture of ions compared to a plasma composed of a single ion species. This is because neutrinos can scatter from concentration fluctuations. The dynamical response function of a heterogeneous plasma is found to have an extra peak at low energies describing the diffusion of concentration fluctuations. Our exact molecular dynamics results for the static structure factor reduce to the Debye Huckel approximation, but only in the limit of very low momentum transfers.

PACS numbers: 26.50.+x, 26.50.+c, 97.60.Jd

I. INTRODUCTION

Core collapse supernovae are extraordinarily energetic explosions where 99% of the energy released is radiated in neutrinos [1, 2]. This is because weakly interacting neutrinos are the only known particles that can diffuse quickly out of the dense stellar core. When the density of the core reaches $\approx 10^{12}$ g/cm³, neutrino nucleus elastic scattering is thought to temporarily trap the neutrinos [3]. The neutrinos then provide a degeneracy pressure that helps support the star. If the neutrinos were not trapped, the star could collapse to a black hole without a large supernova explosion. Thus, the dynamics of a supernova is sensitive to how neutrinos interact in dense matter. For example, changes in the electron capture rate on nuclei could change the sensitive balance between electron Fermi pressure and gravity [4, 5]. However electron capture can only proceed if the produced neutrinos are not Pauli blocked.

The neutrino wave length is comparable to the spacing between ions. Therefore, ion-ion correlations can significantly modify neutrino-nucleus scattering cross sections. An ion in a plasma will be surrounded by a screening cloud of other ions and perhaps electrons. Neutrino interactions with this cloud will, in general, reduce neutrino-nucleus cross sections and increase the neutrino mean free path, see for example [6]. Most calculations of this screening assume a one component plasma composed of a single species of ion, see for example [7]. A first attempt was made in ref. [8] to consider scattering from a plasma including both alpha particles and heavy nuclei. However, this was based on a simple prescription to describe the mixture.

If the plasma has a mixture of species with different ratios of weak to electromagnetic charges then the screening of neutrino reactions can be very different. Neutrinos scatter from fluctuations in the weak charge density. Fluctuations in composition, that change the weak charge density but do not change the (electric) charge density, will feel no electric restoring force. Therefore, these fluctuations may not be screened and can lead to a large change in the neutrino cross section. This was first discussed in connection with ion and electron screening in refs. [9, 10]. Recently Sawyer [11] argued that composition fluctuations for a mixture of ions with different ratios of neutron number N to charge Z can increase the cross section. However Sawyer used the Debye Huckel approximation which is only valid at very low momentum transfers.

In this paper we use molecular dynamics simulations to accurately calculate neutrino scattering cross sections and mean free paths from a dense plasma composed of mixtures of different ions. Section II discusses the mixture of ions expected in supernova plasmas and presents our neutrino scattering formalism, section III describes our simulations, section IV our results and we conclude in section V.

II. FORMALISM

We are interested in neutrino scattering from a dense plasma during the infall phase of a supernova. As the density and temperature rise the rate of nuclear reactions increases dramatically. This should bring the composition of the plasma into nuclear statistical equilibrium (NSE). In NSE all nuclei are in chemical equilibrium so the abundance of a given state is determined by its binding energy and entropy. We first discuss this NSE composition and then describe how to calculate neutrino scattering from this heterogeneous mixture.

‡e-mail: dkberry@indiana.edu

*Electronic address: lcaballe@indiana.edu

†Electronic address: horowitz@indiana.edu

A. Composition

The composition of a plasma in nuclear statistical equilibrium depends on the density, temperature and proton fraction. For given conditions, we expect the most abundant heavy isotope to have a binding energy and entropy that leads to a large free energy. However nuclear reactions can quickly add or subtract nucleons to this most abundant species. Therefore, we expect a distribution of isotopes near the most abundant one. In addition, entropy can favor some light isotopes such as alpha particles and free neutrons. There have been many statistical models that calculate the NSE composition, see for example [12]. Typically, these statistical approaches incorporate detailed binding energy models but only include the interactions between nuclei approximately.

Alternatively, a semi-classical microscopic model described in ref. [13, 14] includes the strong interactions between nucleons in different nuclei in an identical fashion to the interactions between nucleons in a given nucleus. This allows the model to describe not only a plasma of isolated ions but higher density matter where the nuclei merge together to form complex pasta shapes and then uniform nuclear matter.

However, this simple model may not reproduce the binding energy of individual nuclei as well as statistical models. Although the force has been fit to reproduce the binding energy of nuclear matter, the model does not include pairing and shell structure. Comparing the microscopic and statistical models provides some estimate of the possible range in compositions that could be expected.

In the microscopic model, the location of each nucleon is followed in a molecular dynamics simulation. For example, in ref. [14] trajectories for 40,000 nucleons have been calculated by integrating Newton's laws. At any instant in time, the configuration of nucleons is divided into nuclei using the following simple algorithm. A nucleon is said to belong to a given nucleus if it is within a cutoff radius $R_{cut} = 3$ fm of at least one other nucleon in the nucleus. This algorithm uniquely divides a given configuration of many nucleons into a collection of nuclei. The resulting distribution of nuclei will be presented in section IV. However, first we present our neutrino scattering formalism.

B. Neutrino Scattering

In this section we describe how neutrino scattering is modified by ion-ion correlations. The free neutrino-nucleus elastic scattering cross section is

$$d\sigma_0/d\Omega = \frac{G^2 C^2 E_\nu^2 (1 + \cos\theta)}{4\pi^2}. \quad (1)$$

Here G is the Fermi constant, E_ν is the neutrino energy, θ the scattering angle and C is the total weak charge of

a nucleus with charge Z and neutron number N ,

$$C = -2Z \sin^2 \Theta_W + (Z - N)/2, \quad (2)$$

with a Weinberg angle of $\sin^2 \Theta_W = 0.223$. Note that $\sin^2 \Theta_W \approx 0.25$. In the following we approximate $C \approx -N/2$. For a mixture of ions we will use,

$$C = -\frac{1}{2}\langle N \rangle, \quad (3)$$

where the average neutron number $\langle N \rangle$ is,

$$\langle N \rangle = \frac{1}{N_{ion}} \sum_{i=1}^{N_{ion}} N_i, \quad (4)$$

for a system of N_{ion} total ions where the i th ion has neutron number N_i .

Ion correlations can be taken into account by multiplying $d\sigma_0/d\Omega$ by the static structure factor $S(q)$ [15],

$$d\sigma/d\Omega = d\sigma_0/d\Omega S(q). \quad (5)$$

Here q is the momentum transfer and σ_0 is the free cross section. The static structure factor adds coherently the contributions for neutrino scattering from different nuclei, including the relative phases, and can be calculated from,

$$S(\mathbf{q}) = \frac{1}{N_{ion}} \left(\langle \hat{\rho}^\dagger(\mathbf{q}) \hat{\rho}(\mathbf{q}) \rangle - |\langle \hat{\rho}(\mathbf{q}) \rangle|^2 \right), \quad (6)$$

with $\hat{\rho}(\mathbf{q})$ the density operator is given by,

$$\hat{\rho}(\mathbf{q}) = \sum_{i=1}^{N_{ion}} \frac{N_i}{\langle N \rangle} \exp(i\mathbf{q} \cdot \mathbf{r}_i). \quad (7)$$

Note the choice of the normalization $\langle N \rangle$ in Eqs. (3,7) is a somewhat arbitrary convention. We make this choice because one often approximates a mixed system with a single species where all the $N_i = \langle N \rangle$. Alternatively one could replace $\langle N \rangle$ by $\langle N^2 \rangle^{1/2}$ in both Eqs. (3) and (7) with no change in the cross section in Eq. (5). With this second choice $S(q) \rightarrow 1$ at high q .

The transport mean-free path λ is inversely proportional to the transport cross section σ^t , $\lambda = 1/\rho_i \sigma^t$ with ρ_i the ion density. In a medium, the transport cross section σ^t can be obtained by multiplying the free transport cross section

$$\sigma_0^t = \int d\Omega (1 - \cos\theta) d\sigma_0/d\Omega = \frac{2}{3} G^2 C^2 E_\nu^2 / \pi \quad (8)$$

by $\langle S \rangle$,

$$\sigma^t = \sigma_0^t \langle S \rangle, \quad (9)$$

where $\langle S \rangle$ is the angle average of $S(q)$ [6],

$$\langle S(E_\nu, \rho, T) \rangle = \frac{3}{4} \int_{-1}^1 d \cos\theta (1 + \cos\theta) (1 - \cos\theta) S(q(\theta)). \quad (10)$$

Here $q(\theta)^2 = 2E_\nu^2 (1 - \cos\theta)$ and the factor of $(1 + \cos\theta)$ comes from angular dependence of the free cross section, Eq. (1).

C. Debye Huckel Approximation

At very low momentum transfers q the simple Debye Huckel approximation is valid [16]. This provides insight into our full molecular dynamics simulation results. The static structure factor in the Debye Huckel approximation S_q^{DH} is given by [11],

$$S_q^{DH} = \frac{T}{\rho_i \langle N \rangle^2} \sum_{i,j=1}^{N_{ion}} N_i N_j K_{ij}. \quad (11)$$

Here T is the temperature and

$$K_{ij} = \Pi_{ij} - \frac{(\sum_k Z_k \Pi_{ik})(e^2 \sum_l Z_l \Pi_{lj})}{q^2 + q_e^2 + e^2 \sum_{m,n} Z_m Z_n \Pi_{mn}}, \quad (12)$$

where electron screening is describe by $q_e^2 = (4\alpha/\pi)k_F^2$. In the Debye Huckel approximation,

$$\Pi_{ij} = \frac{\delta_{ij} n_i}{T} = \frac{\delta_{ij}}{VT}, \quad (13)$$

where we assume the density of the i th ion is $n_i = 1/V$ with V the system volume. The total ion density is $\rho_i = N_{ion}/V$. Using this expression for Π_{ij} reduces K_{ij} to,

$$K_{ij} = \frac{1}{VT} \left\{ \delta_{ij} - \frac{e^2}{VT} \frac{Z_i Z_j}{q^2 + \kappa^2} \right\}, \quad (14)$$

with $\kappa^2 = \kappa_{ion}^2 + q_e^2$ and

$$\kappa_{ion}^2 = \frac{e^2}{VT} \sum_i Z_i^2. \quad (15)$$

The final result is

$$S_q^{DH} = \frac{\langle Z^2 \rangle}{\langle N \rangle^2} \left\{ \langle \lambda^2 \rangle - \frac{\langle \lambda \rangle^2 \kappa_{ion}^2}{q^2 + \kappa^2} \right\}, \quad (16)$$

where,

$$\langle \lambda^k \rangle = \frac{\sum_i (\frac{N_i}{Z_i})^k Z_i^2}{\sum_i Z_i^2}, \quad (17)$$

for $k = 1, 2$ and,

$$\langle Z^2 \rangle = \frac{1}{N_{ion}} \sum_i Z_i^2. \quad (18)$$

In the $q = 0$ limit, and neglecting electron screening $q_e^2 = 0$, we have

$$S_0^{DH} = \frac{\langle Z^2 \rangle}{\langle N \rangle^2} (\Delta\lambda)^2. \quad (19)$$

Thus the static structure factor depends on the dispersion in the ratio of weak to electromagnetic charge, with $(\Delta\lambda)^2 = \langle \lambda^2 \rangle - \langle \lambda \rangle^2$. Alternatively for a single component plasma, we have

$$S_q^{DH} = \frac{q^2 + q_e^2}{q^2 + \kappa^2}. \quad (20)$$

We compare our full simulation results to the Debye Huckel expression, Eq. (16), in Section IV.

III. SIMULATIONS

In order to calculate the static structure factor, for arbitrary momentum transfer q , we perform molecular dynamics simulations using the Verlet algorithm [17]. For the conditions we consider, the thermal deBroglie wavelength of the ions is much less than the inter-ion spacing so we assume that the ions behave classically. We are interested in momentum transfers much less than the electron Fermi momentum $q \ll k_F$. Therefore, we can describe the interaction between ions with a Yukawa potential [16]:

$$V(i, j) = \frac{Z_i Z_j e^2}{4\pi r_{ij}} e^{-r_{ij}/\lambda_e}, \quad (21)$$

where r_{ij} is the distance between a pair of ions. The electron screening length is $\lambda_e = \pi/(ek_F)$ where the electron Fermi momentum is $k_F = (\rho_e 3\pi^2)^{1/3}$, the electron density is $\rho_e = \langle Z \rangle \rho_i$, and $e^2 = 4\pi\alpha$.

Periodic boundary conditions are used to minimize finite size effects. The distance between ions r_{ij} is then given in terms of the coordinates x, y and z of the i th and j th particles in the form:

$$r_{ij} = \sqrt{[x_i - x_j]^2 + [y_i - y_j]^2 + [z_i - z_j]^2}. \quad (22)$$

Then, the distance used for the periodic boundary condition is:

$$|l| \equiv \min(|l|, L - |l|). \quad (23)$$

Here L is the side of the cubic box V containing the N_{ion} ions, $L = V^{1/3}$. For ion density ρ_i the box volume is $V = N_{ion}/\rho_i$.

We used three different Fortran molecular dynamics programs to do our simulations. The programs are indicated by the author's initials. All the codes use the direct particle-particle method to calculate interactions, where one directly sums the $\frac{1}{2}N(N-1)$ interactions among N ions. Thus the amount of work to do a simulation increases as the square of the number of particles.

The CH and LC codes are serial codes suitable for doing small problems. They were used for MD simulations of 1000 to 4000 ions. The larger 10000 and 40000 ion runs however were too much work for a serial code, so these were done with a parallel program, DB. The 40000 ion mixture run was particularly time-consuming, both because of the 100 fold increase in work per time step over the 4000 ion run, and because it had to be run longer in order to capture the diffusion of the weak charge fluctuation across the larger simulation box. DB uses the MPI (Message Passing Interface) library to pass messages among processes. The N ions are partitioned into p sets, where p is the number of MPI processes, and each process is tasked with calculating the forces on its set of N/p particles due to all N . This makes for $\frac{1}{2}N(N-1)/p$ interactions per process per time step. The main communication needed is for all processes to share their coordinates

with each other, what is called an “allgather”. This can result in a high communication overhead, which is relatively less costly for large problem sizes. After swapping coordinates, the force calculation and integration of Newton’s equations can proceed without communication. The force calculation in each MPI process is additionally parallelized with OpenMP, which is a set of compiler directives used primarily for parallelizing DO loops on multiprocessor shared memory machines.

Run DB1 was done on a 36 node distributed memory parallel computer at Indiana University, the AVIDD-O machine, where each node board has two AMD Opteron processors (Advanced Micro Devices). Each node ran one MPI process consisting of two OpenMP threads. We started with the 40000 ions uniformly and randomly distributed in a simulation box of edge length $L = 822.8$ fm, and with velocities distributed according to a Boltzmann distribution at temperature $T = 1.00$ MeV. We brought the system to equilibrium during the first 7000 warmup steps, with a time step $\Delta t = 25$ fm/c, and then ran a further 252500 measurement steps, with $\Delta t = 50$ fm/c. Every tenth configuration was written to disk. These were used for calculating $S(q, w)$ and $S(q)$. The velocity-Verlet algorithm was used to integrate Newton’s equations. As this algorithm conserves total energy, we rescaled velocities every 1250 time steps in order to maintain the temperature at $T = 1.00$ MeV. We used 4 Opteron nodes (8 processors) for the warmup steps, 8 nodes (16 processors) for the first 65000 measurement time steps, and 10 nodes (20 processors) for the remaining 187500. The program did not have perfect linear speedup with the number of nodes. A 40000 particle problem is actually too small to run efficiently on this number of processors, due to communication overhead. Speedup becomes more linear as the problem size is increased. The full DB1 run consisted of 259500 MD time steps, and took 793 hours spread out over 8 weeks.

We did the 10000 pure ion run DB2 on one dual processor PowerPC970 node in Indiana University’s 42 node IBM JS20 system. For this run we compiled the code to use only the OpenMP capability, as the 2 processors share the board memory. We again started with the ions uniformly and randomly distributed in a simulation box of edge length $L = 518.4$ fm, and with velocities distributed according to a Boltzmann distribution at $T = 1.00$ MeV. We did 8000 warmup steps at $\Delta t = 25$ fm/c, and 24000 more at $\Delta t = 50$ fm/c. We then did 100000 measurement steps at $\Delta t = 50$ fm/c, again writing out every tenth configuration for analysis. Velocities were rescaled every 1250 time steps to maintain the temperature at $T = 1.00$ MeV. The full DB2 run consisted of 132000 MD time steps and took 346 hours spread out over 16 days. We did run DB2 almost simultaneously with DB1, thus running on two processors caused no extra delay.

Finally, we measure the static structure factor $S(q)$ for

value of \mathbf{q} ,

$$\{q_x, q_y, q_z\} = \frac{2\pi}{L}(n_x, n_y, n_z). \quad (24)$$

To minimize finite size effects we chose n_x, n_y, n_z , as integers. We average over directions of \mathbf{q} to improve the statistics. Statistical error bars for codes CH and DB are estimated from the dependence of $S(q)$ on the direction of \mathbf{q} . Statistical error bars for code LC are estimated by dividing the measurement time into a number of separate groups and looking at the variance of $S(q)$ for different groups.

IV. RESULTS

In this section we present results for the static structure factor from full molecular dynamics simulations and compare to the simple Debye Huckel approximation. However first we present results for the plasma composition based either on a simple microscopic model or on a statistical model.

A. Composition

In this subsection we present results for the distribution of charge Z_i and neutron number N_i to be used in our molecular dynamics simulations. We start with conditions considered in ref. [14]: a density of 0.01 nucleons per fm^3 or 1.66×10^{13} g/cm³, a temperature of $T = 1$ MeV and a proton fraction $Y_p = 0.2$. Reference [14] performed a molecular dynamics simulation in the nucleon coordinates with a simple short range nuclear plus Coulomb interaction. The nuclear interaction was fit to reproduce the saturation density and binding energy of nuclear matter.

The final coordinates of a simulation with 40000 nucleons are divided into nuclei by assuming a nucleon belongs to a nucleus if it is within 3 fm of at least one other nucleon in the nucleus. This algorithm produces a collection of about 300 medium mass nuclei with $\langle A \rangle \approx 100$ shown in Fig. 1. In addition there are a few light nuclei with mass $A < 10$ (not shown) and about 10000 free neutrons.

We are interested in the effects of ion-ion correlations so we neglect the free neutrons. Neutrino interactions with these free neutrons are not expected to have large correlation effects. In addition, we also neglect the light nuclei. The light nuclei have small weak and electromagnetic charges, and are expected to play only a small role in neutrino scattering. Furthermore, the light nuclei have larger thermal velocities that require a smaller molecular dynamics time step which slows down the molecular dynamics simulations.

We compare these microscopic results to the statistical model of Botvina et al. [12] which we also show in Fig. 1. For a slightly lower density 10^{13} g/cm³ and the same Y_p and T , the statistical model yields significantly larger

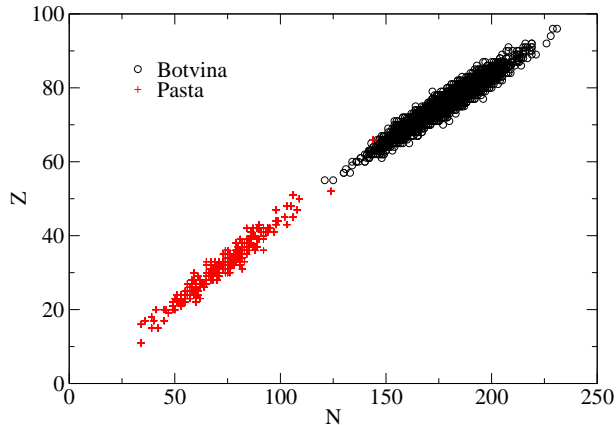


FIG. 1: Distribution of charge Z versus neutron number N for ions at a temperature of $T = 1$ MeV and proton fraction $Y_p = 0.2$. The microscopic Pasta results are from ref. [14] at a density of 1.66×10^{13} g/cm³ while statistical model results are from Botvina et al. [12] at a density of 10^{13} g/cm³.

nuclei $\langle A \rangle \approx 300$. Average $\langle A \rangle$ and $\langle Z \rangle$ are collected in Table I for these two models. The dispersion in the ratio of weak to electromagnetic charge N/Z is important for neutrino scattering. This ratio is plotted in Fig. 2 and the dispersion is more similar for the two models although somewhat larger for the microscopic model.

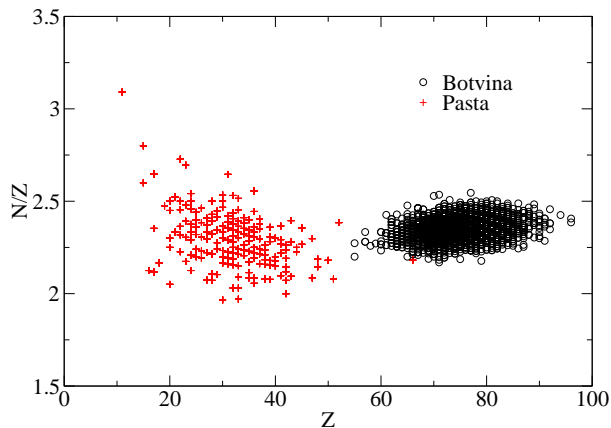


FIG. 2: Ratio of neutron number to charge N/Z versus Z for ions at a temperature of $T = 1$ MeV and proton fraction $Y_p = 0.2$. The microscopic Pasta results are from ref. [14] at a density of 1.66×10^{13} g/cm³ while statistical model results are from Botvina et al. [12] at a density of 10^{13} g/cm³.

TABLE I: Results for ion density ρ_i , average mass number $\langle A \rangle$, average charge $\langle Z \rangle$, and mass fraction of free neutrons X_n for microscopic [14] and statistical [12] models.

Model	ρ (gm/cm ³)	Y_p	ρ_i (fm ⁻³)	$\langle A \rangle$	$\langle Z \rangle$	X_n
Microscopic	1.66×10^{13}	0.2	7.18×10^{-5}	105.2	32.1	0.25
Statistical	10^{13}	0.2	1.60×10^{-5}	328.6	75.7	0.33
Statistical	10^{12}	0.5	1.06×10^{-5}	56.8	28.3	≈ 0

In a core collapse supernova the proton fraction starts out just below $Y_p = 0.5$ and decreases with time due to electron capture. Therefore, in Figs. 3, 4 we show statistical model results for $Y_p = 1/2$, $T = 1$ MeV and a density of 10^{12} g/cm³. Note that the microscopic model has not been simulated for $Y_p = 1/2$. The dispersion in N/Z is smaller for $Y_p = 1/2$ than for $Y_p = 0.2$.

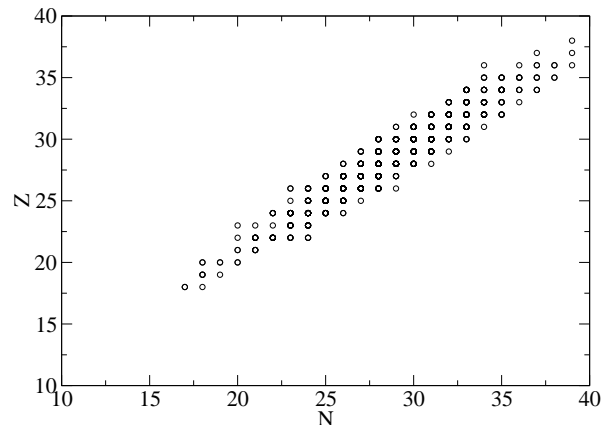


FIG. 3: Distribution of charge Z versus neutron number N for ions in a statistical model [12] at a density of 10^{12} g/cm³, temperature of $T = 1$ MeV and proton fraction $Y_p = 0.5$.

B. Static Structure Factor

In this subsection we present molecular dynamics simulation results for the static structure factor $S(q)$. We ran two simulations with 4000 ions. The first, labeled CH1 in Table II, was based on the mixture in Fig. 1 from the pasta results of [14]. The second, labeled CH2, was for a pure system assuming a single component plasma where each ion has neutron number $N_i = \langle N \rangle$ and charge $Z_i = \langle Z \rangle$ equal to the average values of the mixture. Both simulations were done at density 1.66×10^{13} g/cm³, proton fraction $Y_p = 0.2$, and temperature $T = 1$ MeV. For these conditions the ion density is $\rho_i = 7.18 \times 10^{-5}$ fm⁻³, see Table I. The mixture simulation was started from random coordinates and warmed up for a time of

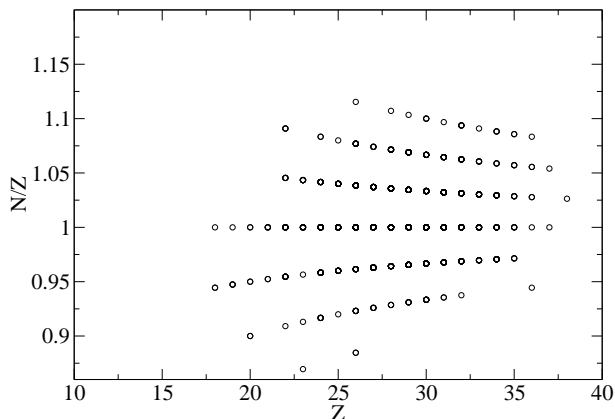


FIG. 4: Ratio of neutron number to charge N/Z versus Z for ions in a statistical model [12] at a density of 10^{12} g/cm³, temperature of $T = 1$ MeV and proton fraction $Y_p = 0.5$.

TABLE II: Simulation runs: the composition is from a microscopic model (Pasta) [14], a statistical model of Botvina (Bot.) [12] or a single (pure) species, the time step is Δt , while T_W is the warm up time and T_M the measurement time, and the potential energy per ion is (V)

Run	N_{ion}	Comp.	Δt fm/c	$\rho_i(10^{-5})$ fm ⁻³	$T_W(10^5)$ fm/c	$T_M(10^6)$ fm/c	(V) (MeV)
CH1	4000	Pasta	50	7.18	5	1.6	367.467(1)
CH2	4000	Pure	50	7.18	1.6	1	368.94(1)
CH3	1000	Bot.	100	1.06	4.1	8	162.952(2)
CH4	1000	Pure	100	1.06	2.4	8	161.990(3)
LC1	1000	Pasta	56	7.18	2.8	1.1	357.65(9)
LC2	1000	Pure	56	7.18	2.8	1.1	359.08(8)
DB1	40000	Pasta	50	7.18	1.8	13	367.712(1)
DB2	10000	Pure	50	7.18	14	5	368.151(1)

500000 fm/c. The system was then evolved for a further 1.6×10^6 fm/c during which $S(q)$ was measured from configurations written to disk every 500 fm/c, see Table II. The pure system was also started from random coordinates, and warmed up for a time of 1.6×10^6 fm/c. It was then evolved for 1.0×10^6 fm/c, with $S(q)$ again measured from configurations written out every 500 fm/c. $S(q)$ for these runs are compared in Fig. 5. In Fig. 6 we compare them for small q , as well as with the Debye Huckel results of Eq. (16).

The first thing we note from these figures is that $S(q)$ for the pure system is systematically smaller than $S(q)$ for the mixture. This is because the mixture can have additional fluctuations in the weak charge density from interchanging isotopes that do not have corresponding fluctuations in the charge density, see below.

Second, Figure 6 shows good agreement between the MD simulation results for $S(q)$ and the Debye Huckel

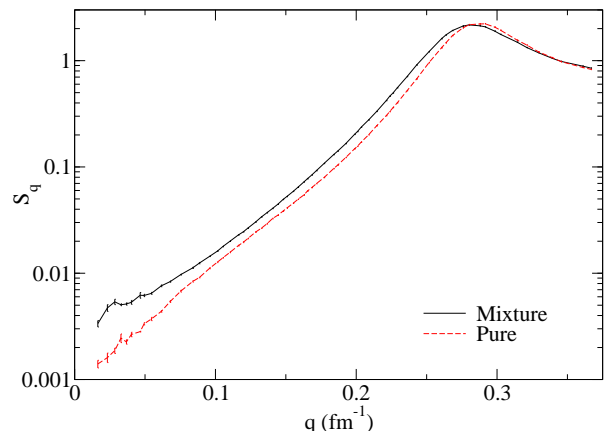


FIG. 5: Static structure factor $S(q)$ versus momentum transfer q for a system at a density of 1.66×10^{13} g/cm³, $Y_p = 0.2$, and $T = 1$ MeV. The solid curve uses a distribution of ions from a microscopic model (CH1) while the dashed line assumes a single component plasma (CH2). Results are from molecular dynamics simulations using 4000 ions. Note the log scale.

approximation S_q^{DH} , Eq. 16, for q between 0.025 and 0.055 fm⁻¹. For $q > 0.055$ fm⁻¹, S_q^{DH} is smaller than $S(q)$ from MD. Therefore, S_q^{DH} is only valid for small q . The lowest q MD result in Fig. 6 corresponds to $q = q_{min} = 2\pi/L$ where L^3 is the simulation volume. There may be a systematic error for this point associated with the finite measurement time of 1.6×10^6 fm/c for the MD calculation of $S(q)$. It may take a long time for fluctuations in the weak charge to diffuse across the system and this may require a long measurement time to obtain an accurate $S(q)$ at low q . We discuss this further in subsection IV D.

We also performed MD simulations comparing the statistical mixture of Botvina against a pure system. These are labeled CH3 and CH4 in Table II, and involve just 1000 ions. Rather using the Botvina distribution shown in Fig. 1, however, where $\rho = 10^{13}$ g/cm³ and $Y_p = 0.2$, we used the mixture of Figs. 3, 4, where $\rho = 10^{12}$ g/cm³ and $Y_p = 0.5$. We kept the temperature at $T = 1$ MeV. The reason is that the denser system may be a solid. The ratio of a typical Coulomb to thermal energy is $\Gamma = Z^2\alpha/aT$ where the ion sphere radius is $a = (3/4\pi\rho_i)^{1/3}$. Assuming a pure system with $Z = \langle Z \rangle = 75.7$ we have $\Gamma = 335$. A pure one component plasma is expected to be a solid for $\Gamma > 180$. Note, the behavior of a mixture of ions could be somewhat different from a pure system. However, given the very large value of Γ the mixture could still solidify.

The $S(q)$ curves of runs CH3 and CH4 are shown in Figs. 7 and 8. Now there is agreement between MD and

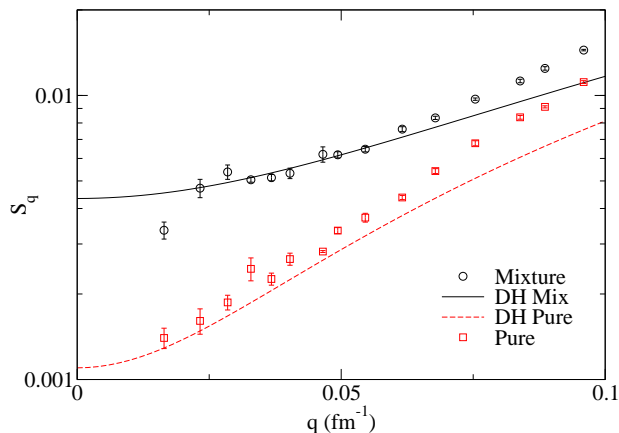


FIG. 6: Detail of the static structure factor $S(q)$ versus momentum transfer q at low q from Fig. 5. Debye Huckel results, Eq. (16) for a mixture of ions are shown as the solid line while the dashed line shows results for a pure system. Note the log scale.

Debye Huckel results near $q \approx 0.015 \text{ fm}^{-1}$. For $Y_p = 0.5$ the spread in N/Z for the ions is smaller than at $Y_p = 0.2$. As a result, $S(q)$ for the mixture is enhanced over $S(q)$ for the pure system by a smaller amount than at $Y_p = 0.2$. These results for $S(q)$ will be used in subsection IVE to calculate neutrino mean free paths. However, first we present results for the dynamical response function to gain insight into the difference between $S(q)$ for mixtures and $S(q)$ for a pure system.

C. Dynamical Response Function

In this subsection we calculate the dynamical response function $S(q, w)$ to study further the difference between pure systems and systems with mixtures of ions. The dynamical response function describes the probability for a neutrino to transfer momentum q and energy w to the system. We have calculated $S(q, w)$ for a microscopic nucleon model in ref. [18]. The static structure factor is the energy integral of $S(q, w)$,

$$S(q) = \int_0^\infty S(q, w) dw. \quad (25)$$

We calculate $S(q, w)$ as an integral over the density-density correlation function $S(q, t)$ as follows,

$$S(q, w) = \frac{1}{\pi} \int_0^{T_{max}} S(q, t) \cos(wt) dt, \quad (26)$$

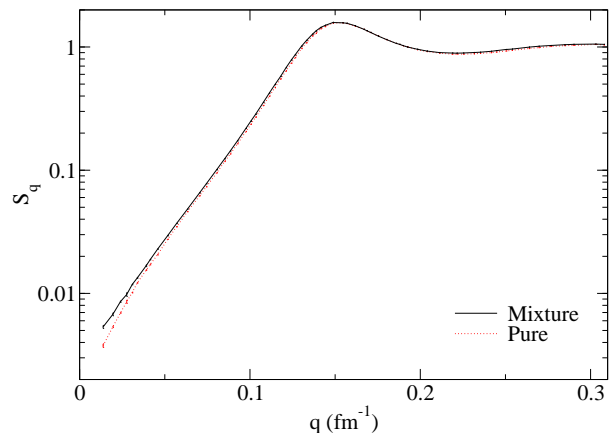


FIG. 7: Static structure factor $S(q)$ versus momentum transfer q for a system at a density of 10^{12} g/cm^3 , $Y_p = 0.5$, and $T = 1 \text{ MeV}$. The solid curve uses a distribution of ions from a statistical model (run CH3) while the dashed line assumes a single component plasma (run CH4). Results are from molecular dynamics simulations using 1000 ions. Note the log scale.

where $S(q, t)$ is,

$$S(q, t) = \frac{1}{N_{ion} T_{ave}} \int_0^{T_{ave}} \rho(q, t+s)^* \rho(q, s) ds. \quad (27)$$

Here $\rho(q, t)$ is $\hat{\rho}(q)$, Eq. (7), evaluated with ion coordinates $r_i(t)$ at time t . We note that $S(q) = S(q, t=0)$. Figure 9 shows $S(q, w)$ for $q = 0.116 \text{ fm}^{-1}$ at a density of $1.66 \times 10^{13} \text{ g/cm}^3$, $Y_p = 0.2$, and $T = 1 \text{ MeV}$, assuming either a mixture of ions from the microscopic model or a single ion species. All simulations show a large peak near $w = 0.003 \text{ fm}^{-1}$ (0.6 MeV) that corresponds to plasma oscillations of the ions [16]. This peak is virtually identical for calculations with a mixture of ions or a single species. Plasma oscillations may depend on the ratio of charge density to average ion mass, since the restoring force depends on the charge density while the oscillation frequency also depends on one over the ion mass. However plasma oscillations do not appear to depend on the dispersion in the ion charge or mass distributions.

In addition, the simulation for a mixture of ions shows a large peak at $w = 0$. This peak is absent in simulations with a single ion species. We conclude that this $w = 0$ peak is the primary difference between mixtures and a single species. The static structure factor of a mixture is larger than $S(q)$ for a pure system by the area under this $w = 0$ peak. Fluctuations in weak charge density, at fixed charge density, feel no electrostatic restoring force. Therefore these fluctuations will diffuse slowly throughout the system and contribute to the response at low w . However, such fluctuations in weak charge concentration are only possible for mixtures. In a pure system the

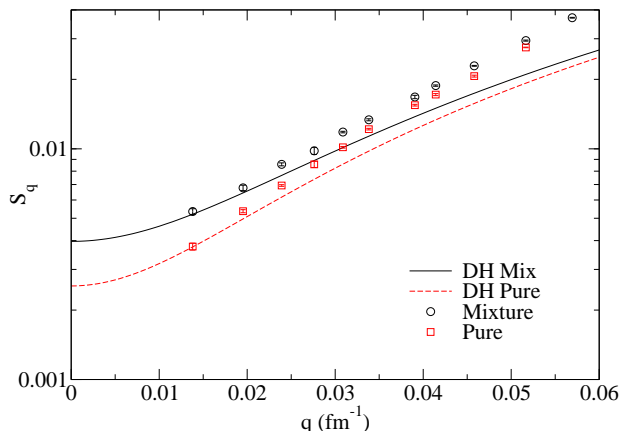


FIG. 8: Detail of the static structure factor $S(q)$ versus momentum transfer q at low q from Fig. 7. The circles are results for a mixture of ions while the squares are for a pure system. Debye Huckel results, Eq. (16) for a mixture of ions are shown as the solid line while the dotted line shows results for a pure system. Note the log scale.

weak charge density must be proportional to the electromagnetic charge density and there can be no weak charge fluctuations without electrostatic restoring forces. Therefore the response of the pure system has no large peak at $w = 0$.

The peak at $w = 0$ is also seen in the microscopic calculations of Ref. [18]. Here molecular dynamics simulations were performed directly in the nucleon coordinates. Nucleons dynamically formed clusters (nuclei) of different N and Z under the influence of nuclear and Coulomb interactions. Fluctuations in concentration of these clusters can then diffuse as in our ion simulations. In addition, these microscopic calculations have two effects that are not in the ion simulations. First, the nuclei have a variety of excited internal modes. Second, nucleons can diffuse into and out of clusters leading to nuclear reactions and the changing of N and Z . These microscopic degrees of freedom may be responsible for significantly broadening the plasma oscillation peak. However, since both the ion and microscopic simulations have the $w = 0$ peak, we conclude that these microscopic degrees of freedom are not necessary for the low energy mode.

Finally, we have calculated $S(q, w)$ for a pure system by approximating the integrals in Eqs. (26,27) by a sum using a time step Δt of 250 or 50 fm/c. In both cases the ion trajectories have been integrated with a time step of 50 fm/c. At high w near 0.005 fm^{-1} the calculation with $\Delta t = 250 \text{ fm/c}$ shows a small but nonzero value. This appears to be a numerical artifact because the response for $\Delta t = 50 \text{ fm/c}$ is much smaller. However, the response at $w = 0$ does not show a peak for either value of Δt .

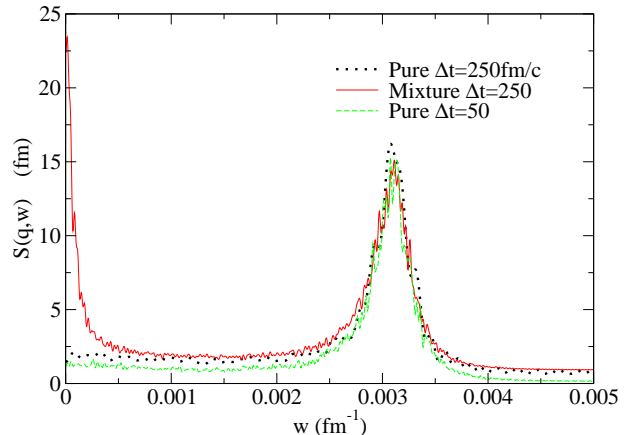


FIG. 9: Dynamical response function $S(q, w)$ versus energy transfer w for $q = 0.116 \text{ fm}^{-1}$ at a density of $1.66 \times 10^{13} \text{ g/cm}^3$, $Y_p = 0.2$ and $T = 1 \text{ MeV}$, from MD simulations with 4000 ions. The solid curve assumes a mix of ions from the microscopic model [14], and has a large peak near $w = 0$. The dotted and dashed curves are for a single component pure system using a time step Δt of either 50 or 250 fm/c (see text).

We conclude that the large $w = 0$ peak seen in the mixture simulation, but not seen in either pure simulation, is unlikely to be a numerical artifact.

D. Finite Size Effects

In this subsection we study the dependence of the MD results on the number of ions in the simulation. In figure 10 we compare $S(q)$ results for simulations using 1000, 4000, and 40000 ions. All simulations are for a mixture of ions at a density of $1.66 \times 10^{13} \text{ g/cm}^3$, as in Fig. 5. For momentum transfers below $q = 0.055 \text{ fm}^{-1}$ there is good agreement between MD simulation results for 40000 ions and the Debye Huckel approximation. However, despite measuring for the relatively long time of $1.3 \times 10^7 \text{ fm/c}$, see run DB1 in Table II, there are still significant statistical errors at the lowest q values. A MD simulation with 4000 ions, see run CH1 of Table II, agrees with the Debye Huckel $S(q)$ (and with run DB1) for $0.02 < q < 0.055 \text{ fm}^{-1}$. However, the smallest q point near 0.017 fm^{-1} is somewhat lower. Finally, a simulation with 1000 ions, see run LC1 of Table II, underpredicts the Debye Huckel $S(q)$ for $q < 0.05 \text{ fm}^{-1}$.

In order to minimize finite size effects, we calculate $S(q)$ for q greater than or equal to a minimum value $q_{min} = 2\pi/L$ with L the box size. This minimum q is clearly smaller for simulations with more ions. However, the relatively large statistical errors found for $S(q)$ at

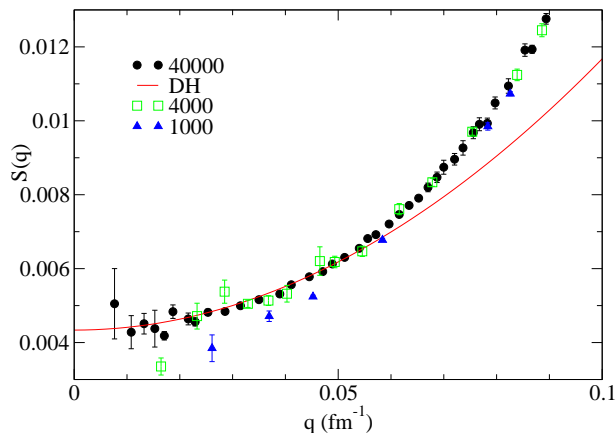


FIG. 10: Static structure factor $S(q)$ versus momentum transfer q for conditions as in Fig. 5 assuming a mixture of ions from a microscopic model [14]. Molecular dynamics results for 1000 ions are solid triangles, 4000 ions are open squares, and results for 40000 ions are filled circles. The solid curve is the Debye Huckel approximation.

small q may be because it takes a long time for concentration fluctuations to diffuse across a large box size L . Therefore, in order to simulate $S(q)$ accurately at small q it appears to be necessary to both use a large number of particles and to measure for a long time. Nevertheless, we conclude from Fig. 10 that molecular dynamics simulation results for $S(q)$ do converge to the Debye Huckel approximation for small q and that this convergence is clearly seen in simulations with 4000 or 40000 ions and for $q < 0.055 \text{ fm}^{-1}$.

Figure 11 shows $S(q)$ for a pure system composed of a single ion species from MD simulations using 1000, 4000, and 10000 ions, see the LC2, CH2, and DB2 runs respectively in Table II. Finite size effects appear smaller than in Fig. 10. For a pure system there are no fluctuations in concentration. Therefore difficulties with large diffusion times and statistical errors both appear reduced at small q . Again the MD results appear to converge to the Debye Huckel approximation, although this convergence may only occur at smaller $q < 0.03 \text{ fm}^{-1}$ compared to the $q < 0.055 \text{ fm}^{-1}$ of Fig. 10.

The agreement between our MD results and the Debye Huckel approximation at low q provides a significant test of our simulation codes. Furthermore three independent MD codes CH (used for runs CH1 through CH4 of Table II, etc.) , DB, and LC were used. There appears to be good agreement between the codes.

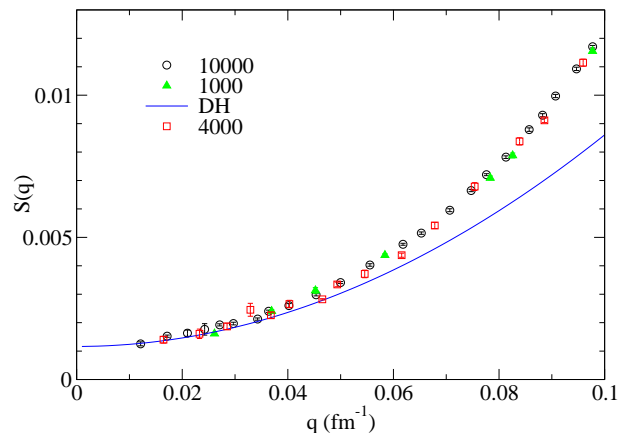


FIG. 11: Static structure factor $S(q)$ versus momentum transfer q for conditions as in Fig. 5 assuming a single ion species. Molecular dynamics results for 1000 ions (triangles), 4000 ions (squares) and 10000 ions (circles) are shown. The solid curve is the Debye Huckel approximation.

E. Neutrino Mean Free Path

In this subsection we use our $S(q)$ results to calculate neutrino scattering mean free paths. Figure 12 shows the neutrino transport mean free path λ (for nucleus elastic scattering) versus neutrino energy at a density of $1.66 \times 10^{13} \text{ g/cm}^3$ based on simulations CH1, and CH2 of Table II. We see that ion-ion correlations significantly increase λ compared to that for free ions.

Next, Fig. 13 shows the ratio of mean free paths from Fig. 12 for a mixture of ions compared to a single ion species. The mean free path for a mixture can be up to a factor of two shorter than that for a pure system.

V. SUMMARY AND CONCLUSIONS

Neutrinos in core collapse supernovae are likely first trapped by large neutrino-nucleus elastic scattering cross sections. These cross sections are reduced by ion-ion correlations. In this paper, we present classical molecular dynamics (MD) simulations of ion systems with strong Coulomb interactions. We find that neutrino cross sections for mixtures of ions, with a dispersion in the ratio of neutron to proton number, are systematically larger than those for a pure system composed of a single ion species. We consider ion compositions from both a microscopic dynamical model and a statistical model.

To investigate the difference between ion mixtures and pure systems we calculate the dynamical response function $S(q, w)$. This describes the probability for a neutrino

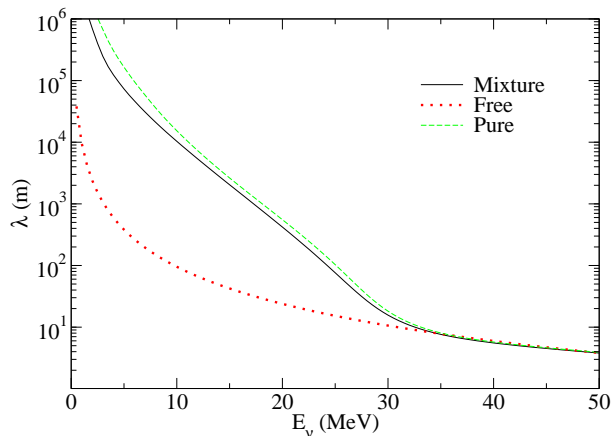


FIG. 12: Neutrino transport mean free path λ versus neutrino energy E_ν at a density of $1.66 \times 10^{13} \text{ g/cm}^3$. The solid curve shows results for a mixture of ions while the dashed curve is for a pure single species of ion. Finally, the dotted curve is for free ions and neglects ion-ion correlations.

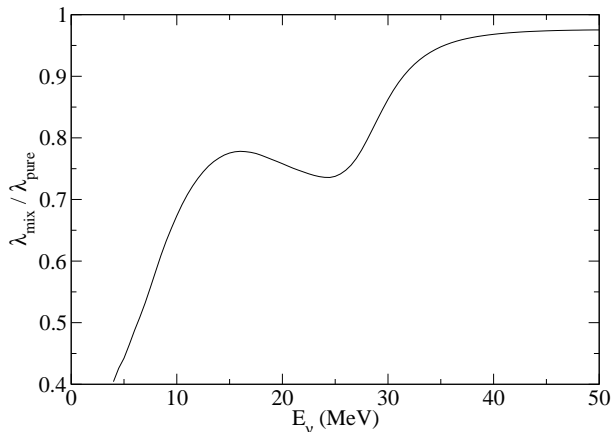


FIG. 13: Ratio of neutrino transport mean free paths versus neutrino energy E_ν for a mixture of ions compared to that for a pure system. Conditions as in Fig. 12.

to transfer momentum q and energy w . We find that mixtures have an extra peak in $S(q, w)$ at $w = 0$ that corresponds to diffusion of composition fluctuations. This peak is absent in simulations of a single ion species.

Our exact MD simulation results for the static structure factor $S(q)$ reduce to the Debye Huckel approximation in the limit of small momentum transfer q . However, this reduction may only happen at very small q . We have studied finite size effects by comparing MD simulations with 1000 to 40000 ions. Finite size effects appear small for 4000 or more ions. However, it may be necessary to measure $S(q)$ for long simulation times in order to obtain accurate results at small q .

Neutrino transport mean free paths can be as much as a factor of two shorter in mixtures compared to a pure system, for low neutrino energies and neutron rich conditions. The dispersion in composition may be smaller in less neutron rich systems. Finally, an important remaining uncertainty is simply the average ion composition predicted by different models. The neutrino mean free path can be significantly influenced by changes in the average nuclear size.

VI. ACKNOWLEDGEMENTS

We thank A. Botvina for providing composition results from his statistical model and R. Sawyer for useful discussion. This work was supported in part by DOE grant DE-FG02-87ER40365 and by Shared University Research grants from IBM, Inc. to Indiana University.

[1] S. Woosley and H.-T. Janka, *Nature Physics* **1** (2005) 147.
 [2] A. Burrows, *Ann. Rev. Nuc. and Part. Sci.* **40** (1990) 181.
 [3] D. Z. Freedman, D. N. Schramm, and D. L. Tubbs, *Ann. Rev. Nucl. Sci.* **27** (1977) 167.

[4] W. R. Hix et al., *Phys. Rev. Lett.* **91** (2003) 201102.
 [5] S. W. Bruenn, A. Mezzacappa, *Phys. Rev. D* **56** (1997) 7529.
 [6] C.J. Horowitz, *Phys. Rev. D* **55**, 4577 (1997).
 [7] N. Itoh, R. Asahara, N. Tomizawa, S. Wanajo, and S. Nozawa, *Astrophys.J.* **611** (2004) 1041.

- [8] A. Marek, H.-Th. Janka, R. Buras, M. Liebendoerfer, M. Rampp, astro-ph/0504291.
- [9] L. B. Leinson, V. N. Oraevsky, and V. B. Semikoz, Phys. Lett. **B209** (1988) 80.
- [10] C. J. Horowitz and K. Wehrberger, Phys. Rev. L. **66** (1991) 272.
- [11] R. F. Sawyer, Phys. Lett. **B630** (2005) 1.
- [12] A. S. Botvina and I. N. Mishustin, Phys. Lett. B **584** (2004) 233.
- [13] C. J. Horowitz, M. A. Perez-Garcia, and J. Piekarewicz, Phys.Rev. **C69** (2004) 045804.
- [14] C.J. Horowitz, M.A. Perez-Garcia, J. Carriere, D. K. Berry, and J. Piekarewicz, Phys.Rev. **C70** (2004) 065806.
- [15] P. Nozieres, Theory of Interacting Fermi Systems (Benjamin, N.Y., 1964),p.53
- [16] A. L. Fetter and J. D. Walecka, Quantum Theory of Many Body Systems (McGraw-Hill, New York,1971).
- [17] F. Ercolessi, A Molecular Dynamics Primer, available from <http://www.sissa.it/furio/> (1997).
- [18] C. J. Horowitz, M.A. Prez-Garca, D. K. Berry, J. Piekarewicz, Phys.Rev. **C72** (2005) 035801.